JOURNAL OF MATERIALS SCIENCE **39** (2004) 3433–3442

Microstructure and its correlation to magnetic properties in 2:17 type (Sm,Gd)-Co-Fe-Cu-Zr alloys

A. C. ABHYANKAR, R. GOPALAN, A. K. SINGH, K. MURALEEDHARAN, V. A. JOSHI, T. S. R. K. SASTRY, V. CHANDRASEKARAN
Defence Metallurgical Research Laboratory, Kanchanbagh, Hyderabad-500 058, India

Studies on the evolution of microstructure and phase transformation at various stages of thermal processing have been carried out in 2:17 type (Sm,Gd)-Co-Fe-Cu-Zr alloys. Microstructural studies reveal that during the solution heat treatment stage, a lamellar structure is formed and its volume fraction is found to be more at 1463 K for alloys without Gd, while at 1473 K for alloys with Gd = 25 wt% of Sm. It appears that the formation of the lamellar structure is closely associated with the phase transformation from $Th_2Ni_{17} \rightarrow (TbCu_7 + Th_2Zn_{17})$ structure during the solution heat treatment. Magnetic measurements in isothermally aged (1123 K) samples showed that the replacement of 25% of Sm by Gd reduces the energy product from 180 to 136 kJ/m^3. The Gd substitution is also found to reduce the temperature coefficient of magnetisation from 350 to 225 ppm/°C in the temperature range of 30–100°C.

1. Introduction

Among the commercially available rare earth permanent magnets, $Sm_2(CoFeCuZr)_{17}$ magnets (2:17 type SmCo) possess a unique combination of magnetic properties [1–3]. A multi-stage heat-treatment process is adopted to generate a fine scale cellular precipitate microstructure, which is responsible for high coercivity [4] and the coercivity mechanism is predominantly by a domain wall pinning process. The microstructure comprises of 2:17 phase cells separated by a thin boundary phase of $SmCo_5$ (1:5 type) with Zr-rich lamellae running across many cells and cell boundaries [5–9].

For certain applications, where a reduced or near-zero temperature dependence of magnetic flux is required, 2:17 SmCo magnets with partial substitution of heavy rare earth elements (HRE) such as Gd or Er are recommended [10–12]. Walmer *et al.* [12] have studied the magnetic properties of $(Sm_{1-x}Gd_x)_2(Co_{bal}Fe_{.23}Cu_{.06}Zr_{.02})_{17}$ alloys with $x = 0$ to 1 at room temperature and 300°C and determined the composition and temperature dependence of Br, $_iH_c$ and $(BH)_{max}$. The values of Br, $_iH_c$ and $(BH)_{max}$ decrease with increase in Gd content at room temperature. The increase in room temperature from 250 to 300°C also reduces the values of Br, $_iH_c$ and $(BH)_{max}$. It is to be noted that Walmer *et al.* [12] have carried out limited microstructural studies and did not correlated microstructure with magnetic properties.

When a heavy rare earth element is substituted, the negative temperature coefficient of Sm is internally compensated by the positive temperature coefficient of the heavy rare earth element, thereby giving a low temperature coefficient of magnetisation and hence an almost constant level of magnetic flux over a given range of temperature. However HRE substitution reduces the saturation magnetisation of the alloy system and therefore, based on the requirement of magnetic characteristics, a particular combination of Sm and HRE composition is selected. The addition of Gd does not alter the metallurgical transformations due to the chemical similarity between Sm and Gd and hence a similar multistage heat-treatment schedule is also adopted in the Gd-substituted system. The structure-property correlation in 2:17 type SmCo alloys is very interesting and is still a topic of research, particularly with the advent of new high temperature grades [13].

In this paper, the metallurgical and magnetic characterizations carried out on two alloys with nominal compositions (wt%) of 25Sm-52.5Co-15Fe-4.5Cu-3Zr and 18Sm-7Gd-52.5Co-15Fe-4.5Cu-3Zr have been discussed. It is important to mention here that the alloy composition considered in the present study is different from the alloys considered by Walmer *et al.* [12] in terms of Gd as well as other alloying elements. For the sake of discussion of the results in the present study the two experimental alloys are referred to as normal 2:17 and Gd-substituted 2:17. An attempt has also been made to establish a relationship between the microstructure and magnetic properties of the alloys.

2. Experimental

Two alloys with nominal composition (wt%) of 25 Sm-52.5Co-5Fe-4.5Cu-3Zr-18Sm-7Gd-52.5Co-15 Fe-4.5Cu-3Zr were prepared from high purity

(>99.5%) constituent elements by melting in argon. The chemical composition of the alloys was determined by inductively coupled plasma (ICP) as well as by SEM-EDS techniques.

The ingots were crushed and milled to 5–10 μm. A magnetic field >1500 kA/m was used to align the powders and cylindrical samples were die-pressed. The green compacts were sintered and solution heat treated at 1448–1488 K and subsequently subjected to isothermal aging at 1123 K for 12 h followed by slow cooling to 673 K at the rate of 30 K/h.

X-ray diffraction (XRD) patterns were obtained using a Philips X-ray powder diffractometer, PW3020 with Cu K_α radiation. Differential thermal analysis (DTA) studies were carried out using SETARAM setsys TG DTA18 to know the melting point of the constituent phases present in the as-cast alloys. Microstructural investigations were carried out using optical, scanning electron microscope with energy dispersive spectroscope facility (SEM-EDS) (Leo 440i SEM) and electron probe micro analysis (EPMA) [CAMECA Analyzer (CAMEBAX-MICRO)]. Magnetic measurements were performed on cylindrical samples using an auto hysteresis graph (Walker Scientific Inc). The reversible temperature coefficient of magnetisation is measured using a vibrating sample magnetometer (VSM) (Digital Measurement System) on samples subjected to thermal stabilization at 200°C.

3. Results and discussions

3.1. Studies on as-cast alloys

Differential thermal analysis (DTA) curves of as-cast alloys are shown in Fig. 1. The DTA curves reveal the existence of three endothermic peaks in both the alloys. These peaks correspond to the melting point of the constituent phases present in the alloys. It can be seen that the melting point of the phases in Gd substituted alloys is higher by 7–10 K to that of the normal 2:17 alloys. This can be attributed to the higher melting point of Gd to that of Sm. Microstructural studies revealed that these phases correspond to the 2:17 matrix phase (primary crystallites), 1:5 boundary phase and a needle like Zr-rich phase (Fig. 2).

Microstructural studies on the as-cast normal 2:17 alloy at different regions of the ingot showed a homogeneous distribution of phases as illustrated in Fig. 3. A similar microstructural distribution is also found in the Gd-substituted alloy.

The comparison of the compositions (wt%) between ICP and SEM-EDS analysis is given in the Table I along with the nominal composition of the alloys. EPMA analysis was carried out on the as cast alloy to determine the composition of the matrix, boundary and platelet phases and are listed in Table II. The boundary phase, which is rich in Sm, has the composition close to that of the 1:5 type phase. Zr-line profile analysis shown in Fig. 4 indicates that the needle like structure in the boundary phase is a Zr-rich type. It is reported that composition of the Zr-rich needle phase in the cast alloy will be very close to that in fully processed samples and in the present study a similar observation has been made [14].

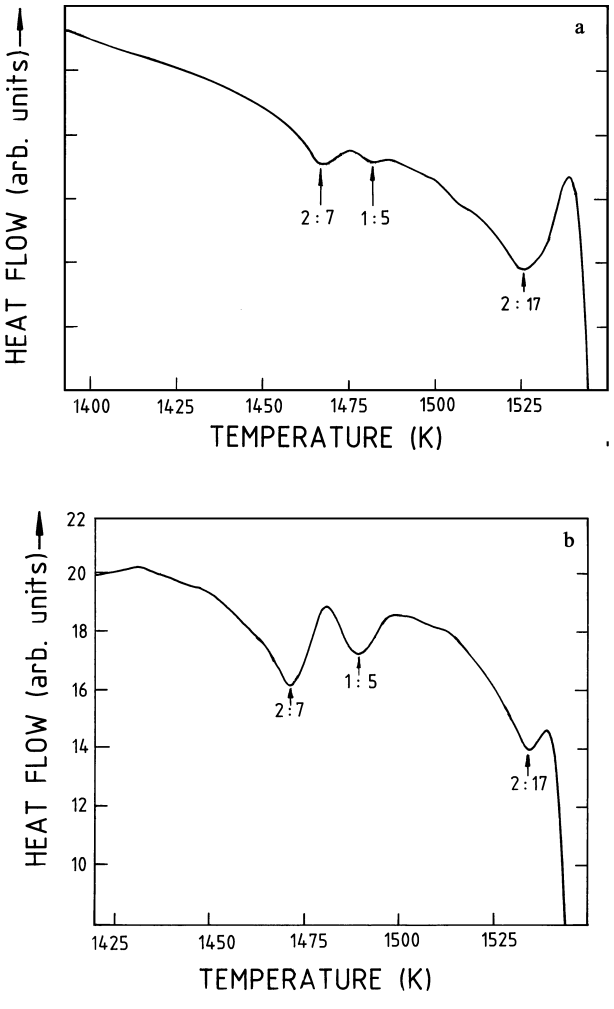

Figure 1 Differential thermal analysis traces of as-cast: (a) normal 2:17 alloy and (b) Gd-substituted 2:17 alloy. Three endothermic peaks can be seen in both the alloys.

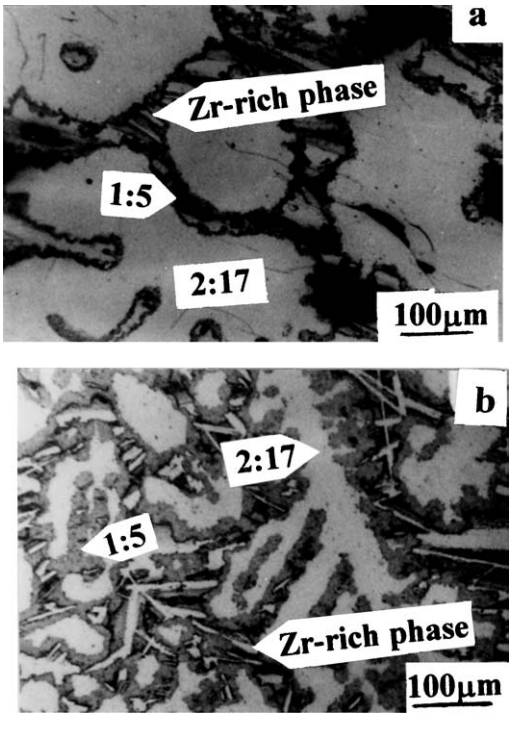

Figure 2 As-cast microstructures of (a) normal 2:17 alloy and (b) Gd-substituted 2:17 alloy. Microstructures reveal the presence of three phases in both the alloys.

TABLE I Compositions of normal 2:17 and Gd- substituted 2:17 alloys obtained by ICP and SEM-EDS techniques

	Composition (wt%)										
	Normal 2:17 alloy					Gd-substituted 2:17 alloy					
	Sm	Co	Fe	Cu	Zr	Sm	Gd	Co	Fe	Cu	Zr
Nominal	25.0	52.5	15.0	4.5	3.0	18.0	7.0	52.5	15.0	4.5	3.0
ICP	25.1	52.7	14.8	4.3	3.1	18.2	7.1	52.3	15.1	4.6	2.7
SEM-EDS	24.8	52.1	15.2	4.6	3.3	18.9	6.6	51.9	15.1	4.9	2.4

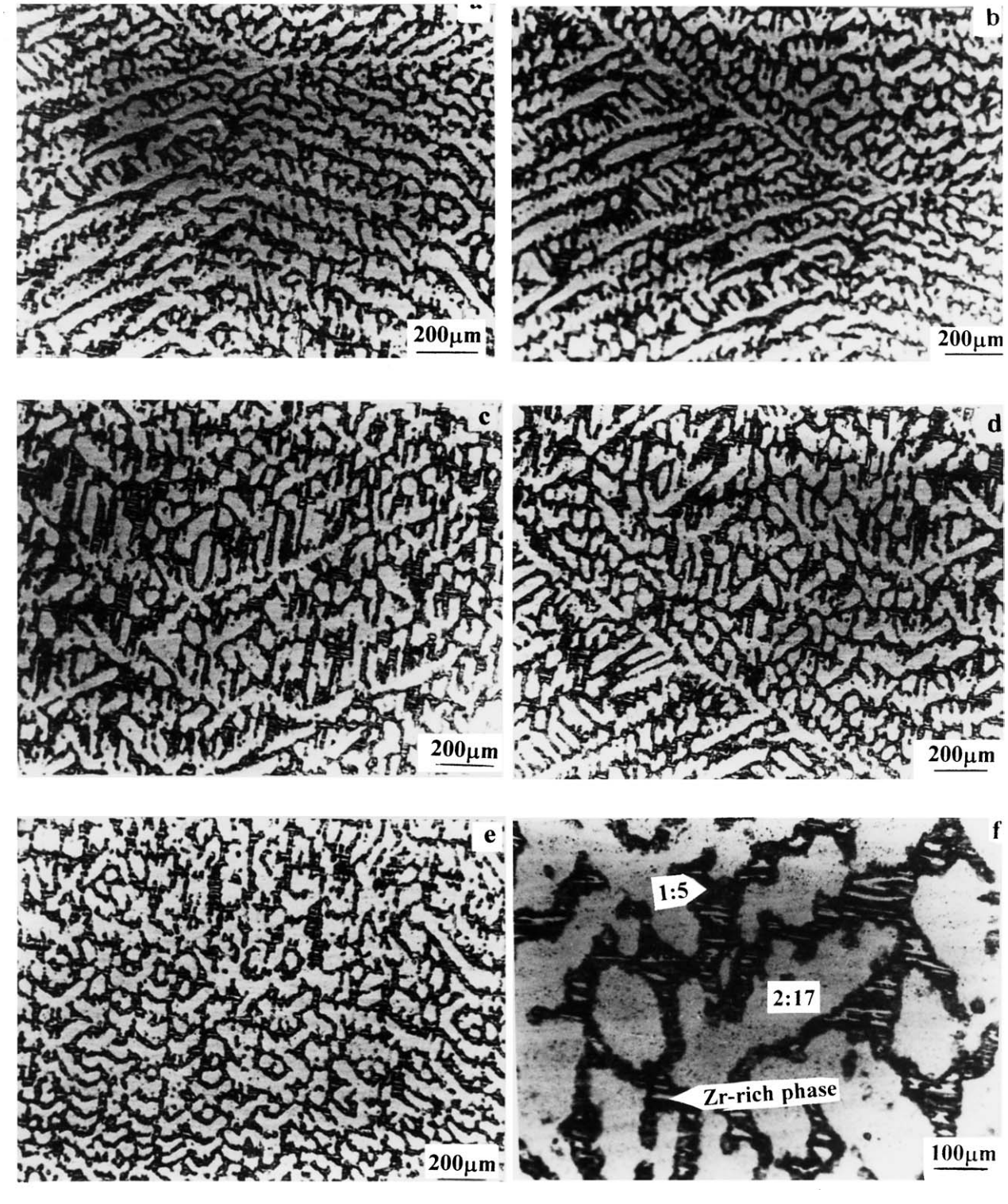

Figure 3 As-cast microstructures of normal 2:17 alloy taken at various regions of the ingot. It can be seen that the microstructure is uniform in all the regions.

TABLE II EPMA analysis of the phases present in as-cast normal 2:17 alloy

Phases	Composition (wt%)				
	Sm	Co	Fe	Cu	Zr
2:17 type matrix phase	23.6	54.1	18.0	3.2	1.1
1:5 type boundary phase	40.6	34.5	7.8	16.1	1.0
Needle like phase	17.1	50.1	10.8	2.9	19.1

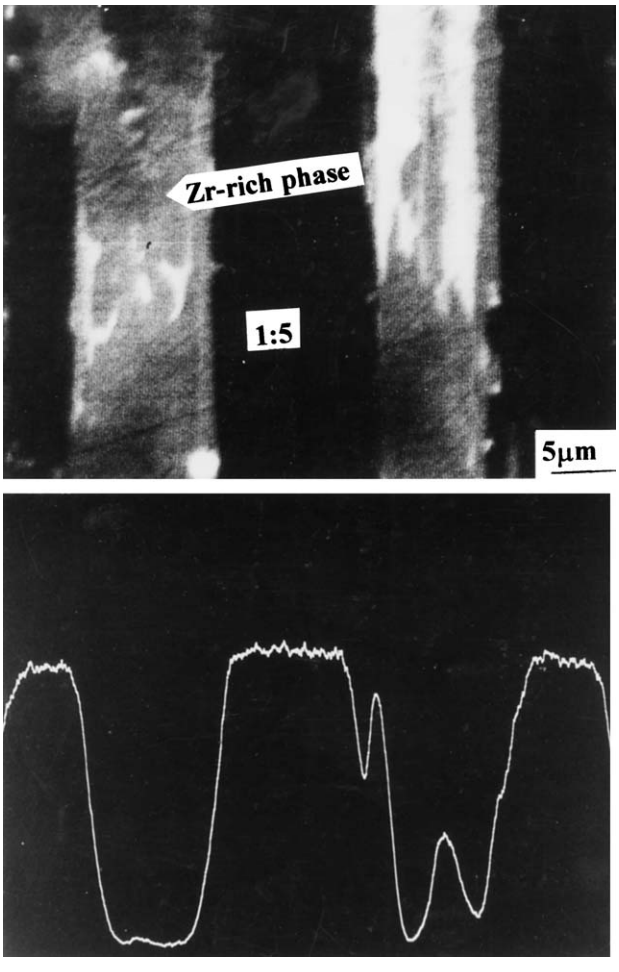

Figure 4 EPMA line profile analysis for Zr-rich needle structure embedded in 1:5 type boundary phase of normal 2:17 alloy.

3.2. Studies on solution heat treated samples

3.2.1. XRD results

The Sm_2Co_{17} phase has three different types of crystal structure viz. (i) hexagonal Th_2Ni_{17} (2:17H), (ii) rhombohedral Th_2Zn_{17} (2:17R) and (iii) hexagonal $TbCu_7$ (1:7H), all derived from $CaCu_5$ type [15]. The formation of these structures in the 2:17 phase can be identified from XRD patterns (Fig. 5). The presence of the (203) and (204) peaks represents 2:17H and 2:17R phases respectively while the absence of both the peaks provides evidence for the formation of the 1:7H phase. It has been reported that the formation of the 1:7H structure at the solution heat treatment stage is essential for the development of large intrinsic coercivities ($_iH_c$) and is attributed to the larger anisotropy of the 1:7H structure [16]. Therefore, it is of scientific and technological importance to study its formation as a function of solution heat treatment temperature in the normal 2:17 and in the Gd-substituted samples.

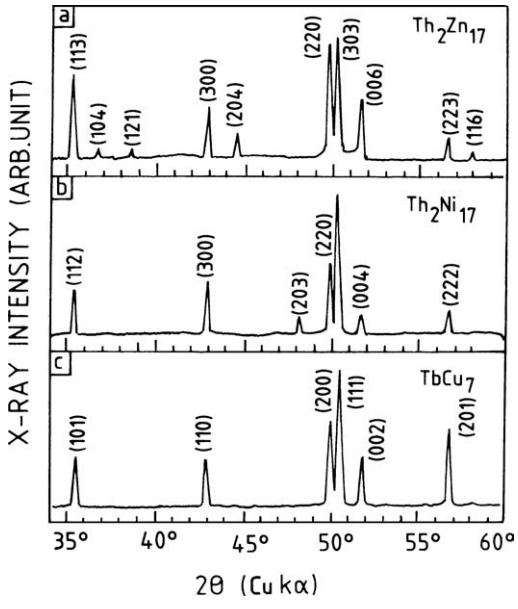

Figure 5 XRD patterns of 2:17 phase with three different crystal structure types, viz. Th_2Zn_{17}, Th_2Ni_{17} and $TbCu_7$ [13].

XRD patterns of normal 2:17 and Gd-substituted 2:17 samples for various solution heat treatments in the temperature range of 1448–1483 K are shown in Figs 6 and 7 respectively. It can be seen that the crystal structure type of the 2:17 phase changes from (1:7H + 2:17R) to (2:17R + 2:17H) at temperatures >1463 K in the case of the normal 2:17 sample and >1473 K for the Gd substituted samples. Prior to the solution heat treatment, the samples exhibit the presence of the 2:17H structure when sintered in the temperature range of 1488–1493 K. An attempt has been made to quantify the fraction of the 2:17R and 2:17H phases present by estimating the ratio of integrated intensity of $(204)_{2:17R}$ to $(203)_{2:17H}$ reflections as a function of the solution heat treatment temperatures. Thus, analysis of the individual XRD patterns for the intensity calculation has been taken into account in determining the ratio $(204)_{2:17R}/(203)_{2:17H}$ as a function of solutionising temperature. This is illustrated in Fig. 8a and b for the normal 2:17 and for the Gd substituted samples respectively. It is clear from Fig. 8 that the solution heat treatment temperatures of 1463 K for the normal 2:17 and 1473 K for the Gd-substituted 2:17 samples result in a small volume fraction of the 2:17H structure.

3.2.2. Microstructural investigations

Understanding the microstructural evolution at the various stages of the heat treatment (sintering, solution heat treatment, isothermal aging and slow cooling) is an important part of studies of the development of 2:17 type SmCo magnets. It is also of interest to investigate the microstructural variations in 2:17 alloys when a heavy rare earth element such as Gd is substituted. As the solution heat treatment stage brings out an important

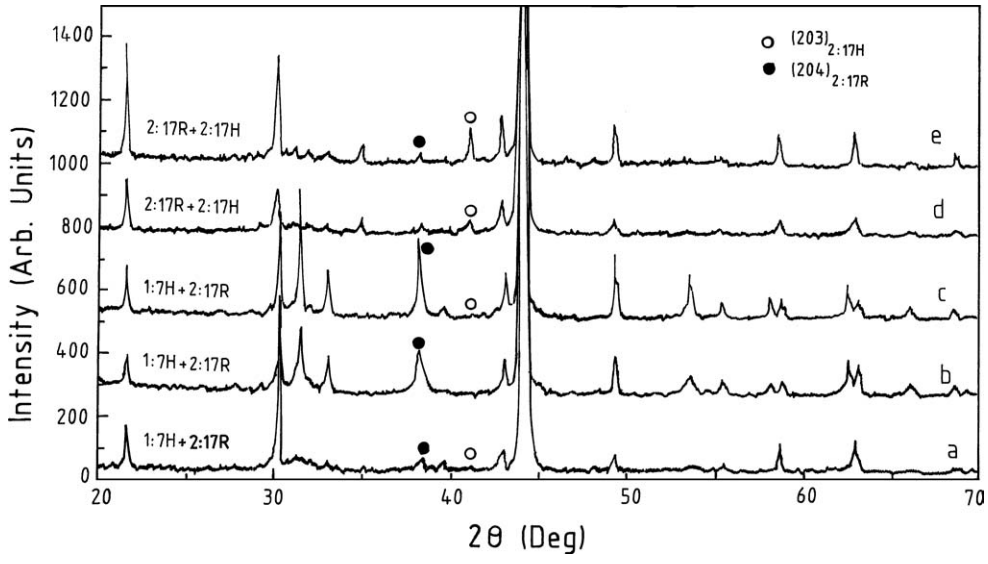

Figure 6 XRD patterns of normal 2:17 samples in sintered and solution heat treated conditions: (a) 1483 K, (b) 1473 K, (c) 1463 K, (d) 1458 K, and (e) 1448 K.

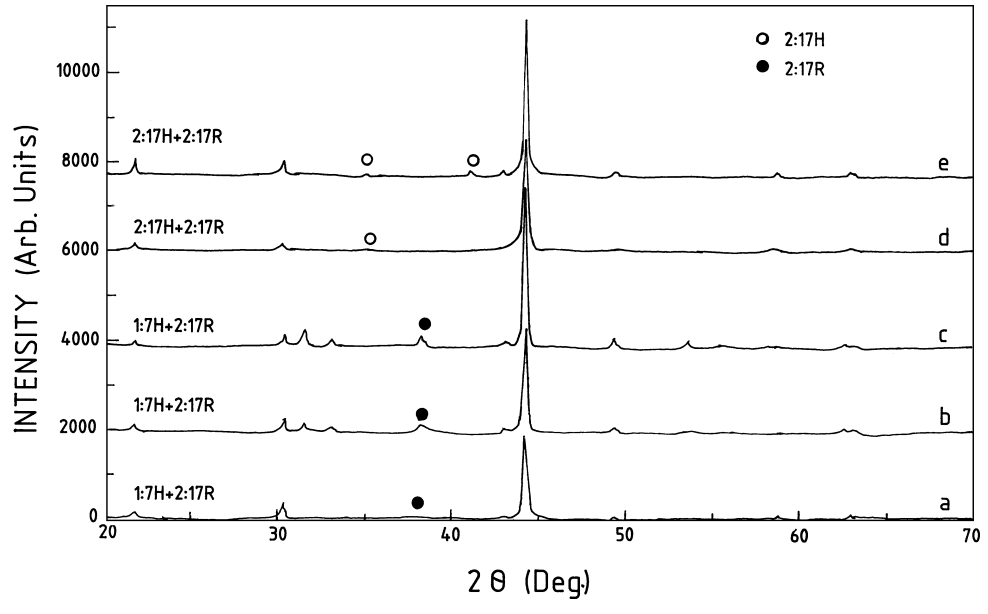

Figure 7 XRD patterns of Gd-substituted 2:17 samples in sintered and solution heat treated conditions: (a) 1488 K, (b) 1473 K, (c) 1468 K, (d) 1463 K, and (e) 1453 K.

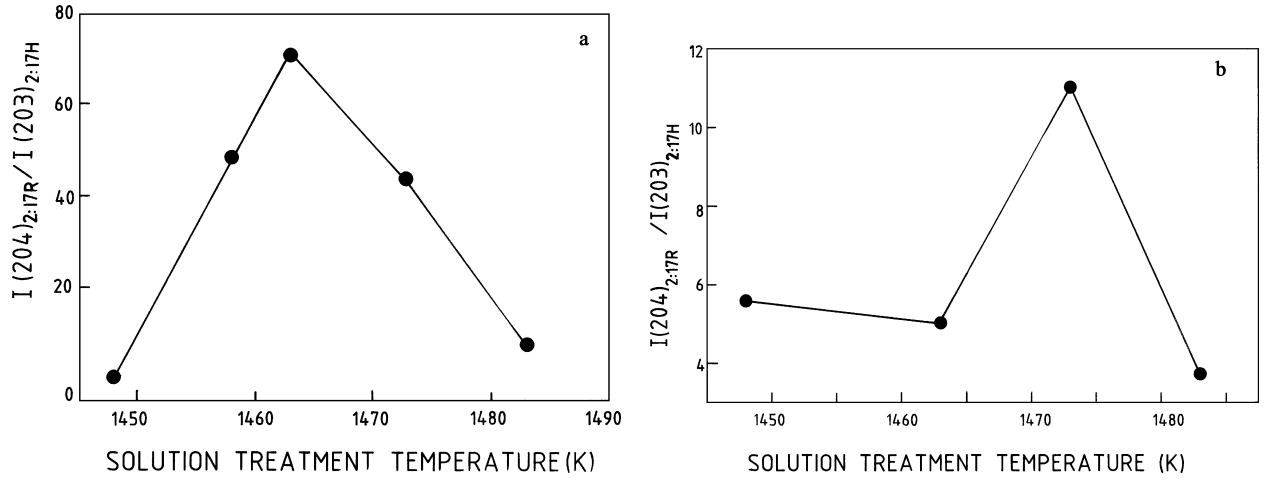

Figure 8 Plots of XRD intensity ratio of $(204)_{2:17R}/(203)_{2:17H}$ as a function of solution heat treatment temperatures for (a) normal 2:17 and (b) Gd-substituted 2:17 samples. It can be seen that the ratio peaks at 1463 K for normal 2:17 and at 1473 K for Gd-substituted 2:17 samples.

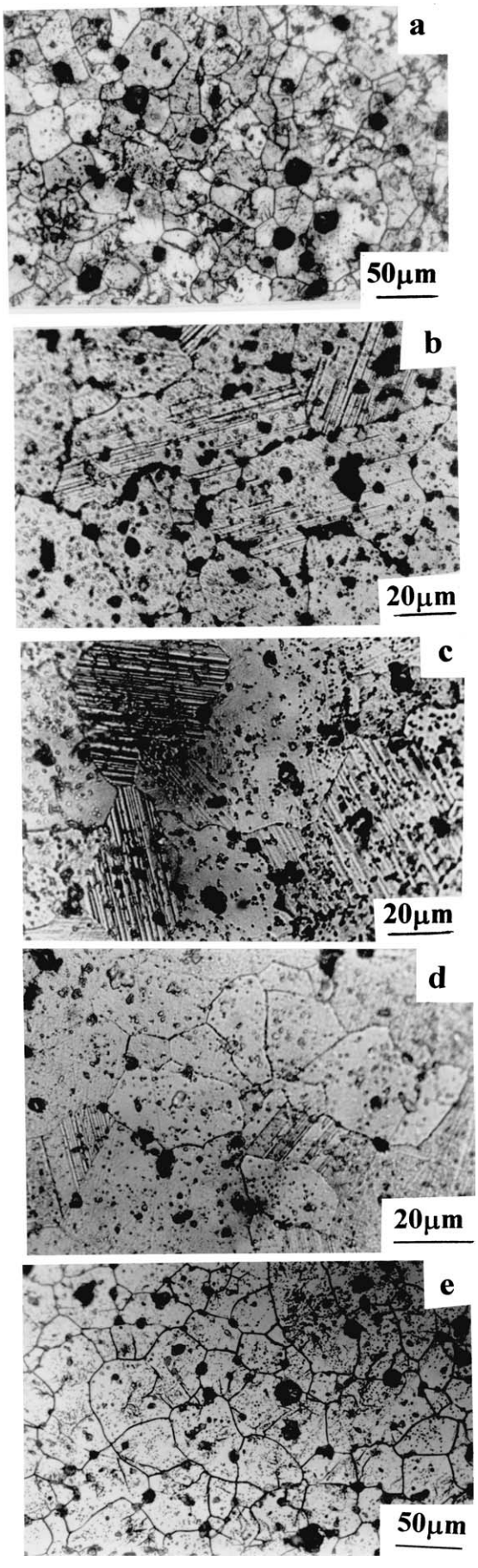

Figure 9 Microstructures of normal 2:17 samples solution heat treated at (a) 1483 K, (b) 1473 K, (c) 1463 K, (d) 1458 K, and (e) 1448 K. Presence of lamellar structure is seen in many of the 2:17 grains for samples solution heat treated at 1463 K.

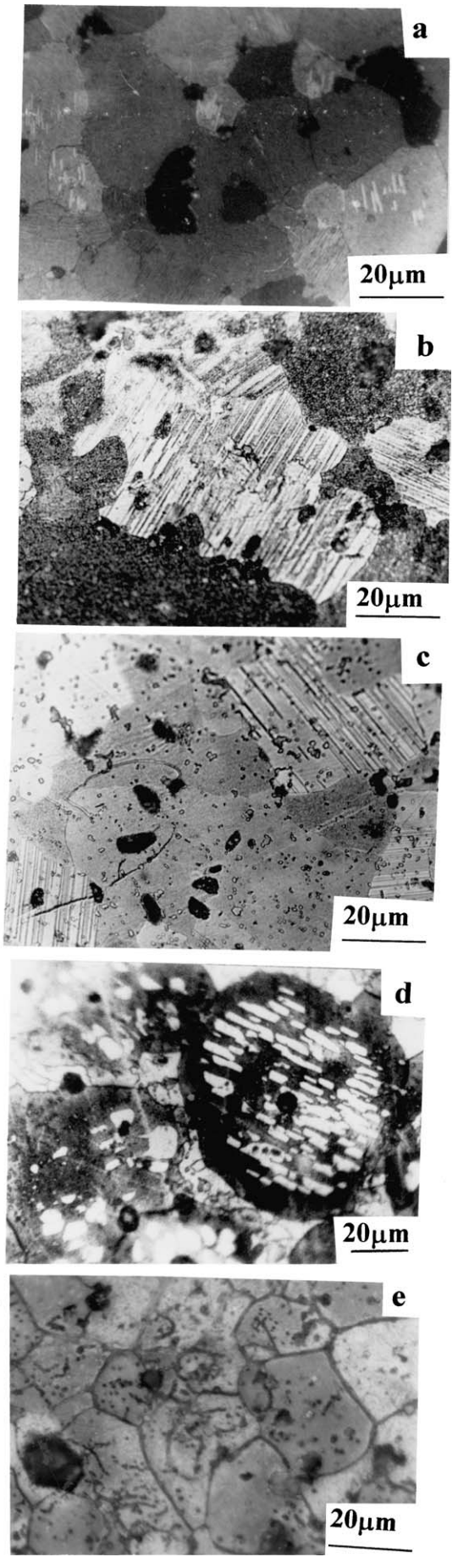

Figure 10 Microstructures of Gd-substituted 2:17 samples solution heat treated at (a) 1488 K, (b) 1473 K, (c) 1468 K, (d) 1463 K, and (e) 1453 K.

structural transformation, viz. 2:17H → 1:7H or 1:7H + partially transformed 2:17R, it is useful to study the microstructural variations as a function of the solution heat treatment temperature.

Figs 9 and 10 show the microstructures of the normal 2:17 and Gd-substituted 2:17 samples respectively for various solution heat treatment temperatures. It can be seen clearly from the Figs 9 and 10 that there is a variation in the density of the lamellar features as the solution heat treatment temperature is varied. It is found that the volume fraction of the lamellae is more at 1463 K for normal 2:17 samples than that at 1473 K for the Gd-substituted sample. It has also been observed that samples solution heat treated below these temperatures exhibit either less or no lamellae. The formation of the lamellar microstructure could be the result of the transformation of the 1:7H + partially transformed 2:17R phase from the high temperature 2:17H phase. This observation also agrees with the results of the XRD analysis shown in Figs 4 and 5. Upon isothermal aging at 1123 K and ramp cooling to 673 K, the proportion lamellar structure observed in the solution heat treated stage becomes greater in both the normal 2:17 as well as in the Gd-substituted samples (Fig. 11a and b).

3.3. Magnetic characterization

3.3.1. Second quadrant characteristics

After isothermal aging and slow cooling (solution heat treated at different temperatures) the samples have been magnetized to saturation in a pulse magnetic field of 6400 kA/m and the second quadrant characteristics determined. While all the samples exhibited an intrinsic coercivity of >1300 kA/m, a systematic variation in the knee field H_k, coercivity H_c, and energy product $(BH)_{max}$ is observed as a function of the solution

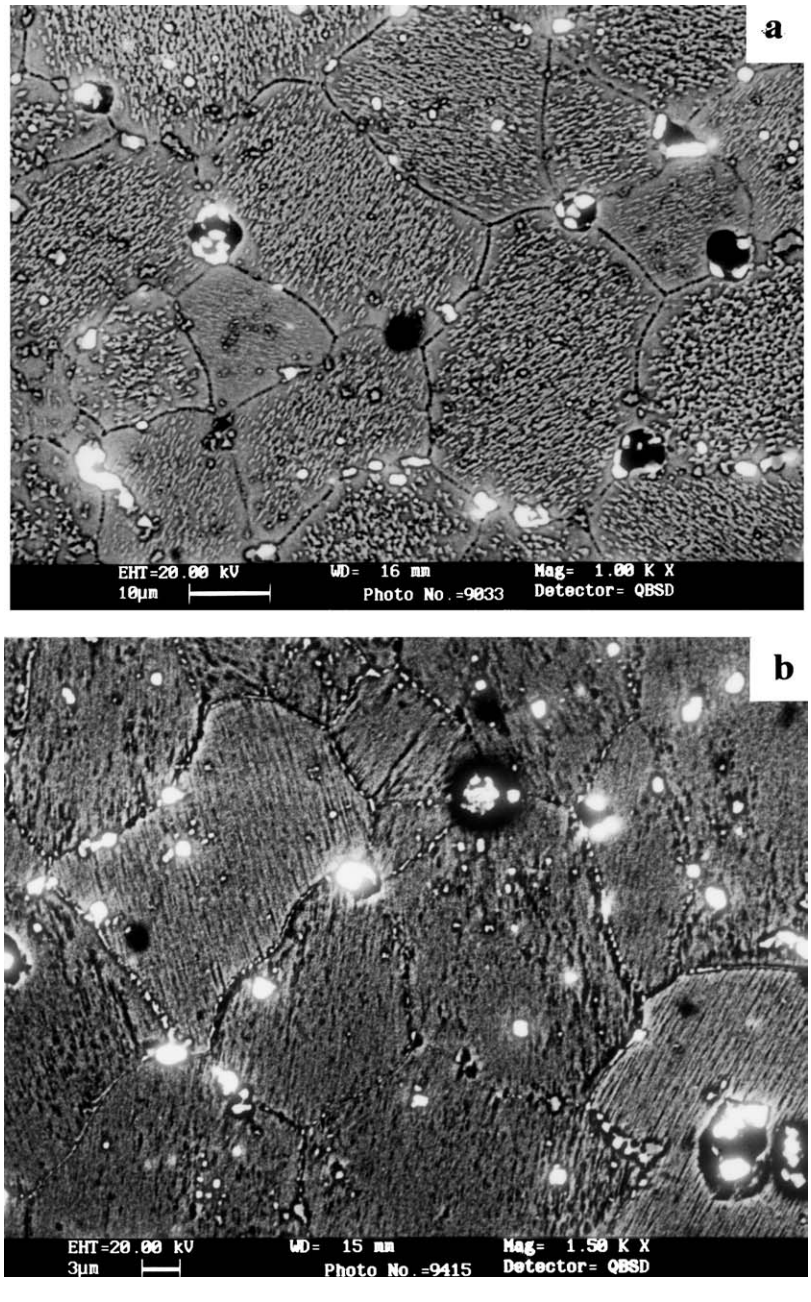

Figure 11 Scanning electron micrographs showing dense lamellar structure in isothermally aged and slow cooled sample of (a) normal 2:17 and (b) Gd-substituted 2:17.

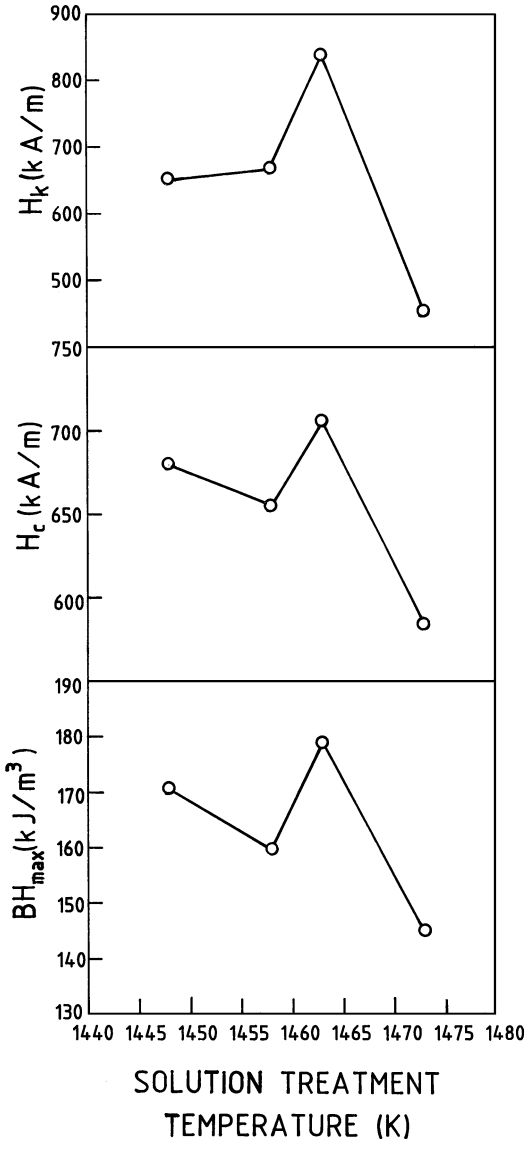

Figure 12 Plots illustrating the variation of magnetic properties [H_k, H_c and $(BH)_{max}$] as a function of solution heat treatment temperature for normal 2:17 samples. The properties peak at 1463 K.

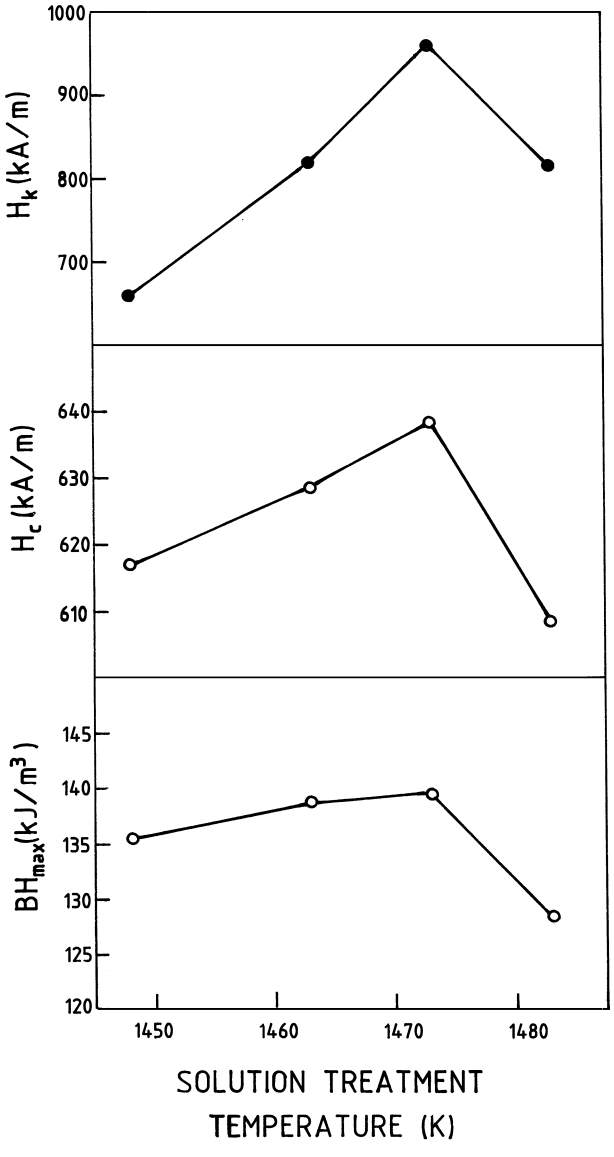

Figure 13 Plots illustrating the variation of magnetic properties [H_k, H_c and $(BH)_{max}$] as a function of solution heat treatment temperature for Gd-substituted 2:17 samples. The properties peak at 1473 K.

heat treatment temperature for both the normal and Gd-substituted 2:17 samples (Figs 12 and 13). It can be seen from the plots that the magnetic properties show a maximum at 1463 K for the normal 2:17 and at 1473 K for the Gd substituted samples. Since $H_k/{}_iH_c$ can be taken as a measure of the squareness ratio of the demagnetization curve, which also represents the effectiveness of domain wall pinning by microstructural features, an attempt has been made to plot the $H_k/{}_iH_c$ ratio as a function of the solution heat treatment temperature (Fig. 14a and b). It can be seen that this ratio exhibits a maxima at 1463 and 1473 K for normal 2:17 and Gd-substituted 2:17 samples respectively. This observation is similar to the variation of XRD intensity ratio for different solution heat treatment temperatures (Fig. 8) and suggests a strong correlation between the structure and the magnetic properties.

Substitution of Gd by 25 wt% has resulted in the reduction of the energy product from 180 to 136 kJ/m^3. However, it is interesting to note that the high ${}_iH_c$ (>1300 kA/m) is retained by the partial replacement of Sm by Gd.

3.3.2. Temperature coefficient of magnetisation

A Vibrating Sample Magnetometer was used to measure the temperature coefficient of the magnetisation. The studies were conducted on those samples which showed ${}_iH_c > 1300$ kAm^{-1}. A small rectangular piece (~100 mg) was cut from the thermally stabilised magnet with the larger dimension of the sample parallel to the direction of magnetisation. Starting from 30°C, the sample was heated to 200°C in steps of 10°C and at each temperature, the magnetisation was measured. The experiment was also repeated for the cooling cycle. It is observed that the magnetisation values were reversible and showed a linear variation both in the heating and cooling cycle. The magnetisation value as a function of temperature is shown in Fig. 15a and b. The average temperature coefficient of the magnetization was evaluated from the formula [18]:

$$\text{Temperature coefficient of magnetisation} = \frac{(P2 - P1)}{P1(T2 - T1)} \times 10^6 \text{ (ppm/°C)}$$

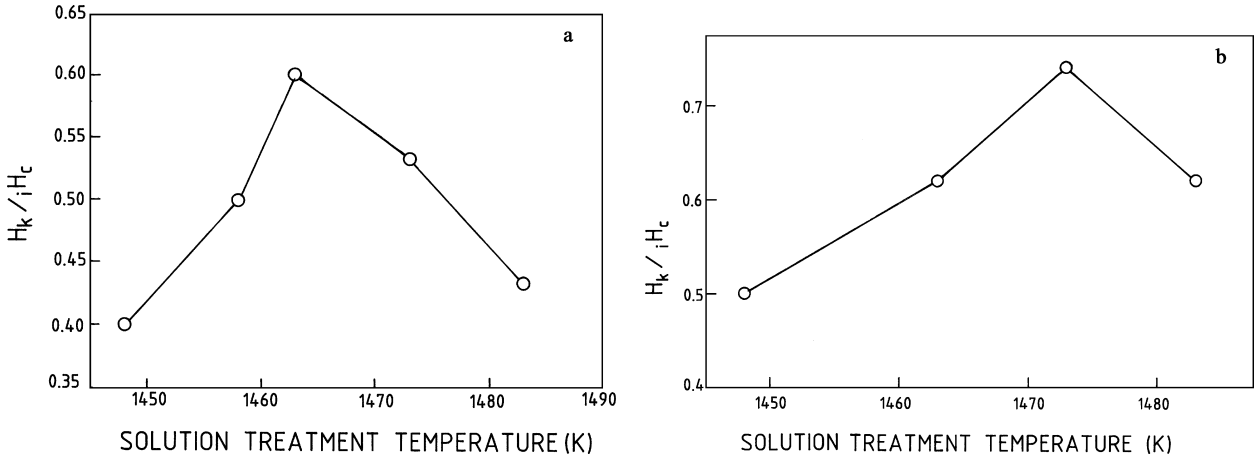

Figure 14 Plots showing the variation of $[H_k/{}_iH_c$ ratio as a function of solution heat treatment temperature for (a) normal 2:17 and (b) Gd-substituted 2:17 samples. The ratio peaks at 1463 and 1473 K for normal 2:17 and Gd-substituted samples.

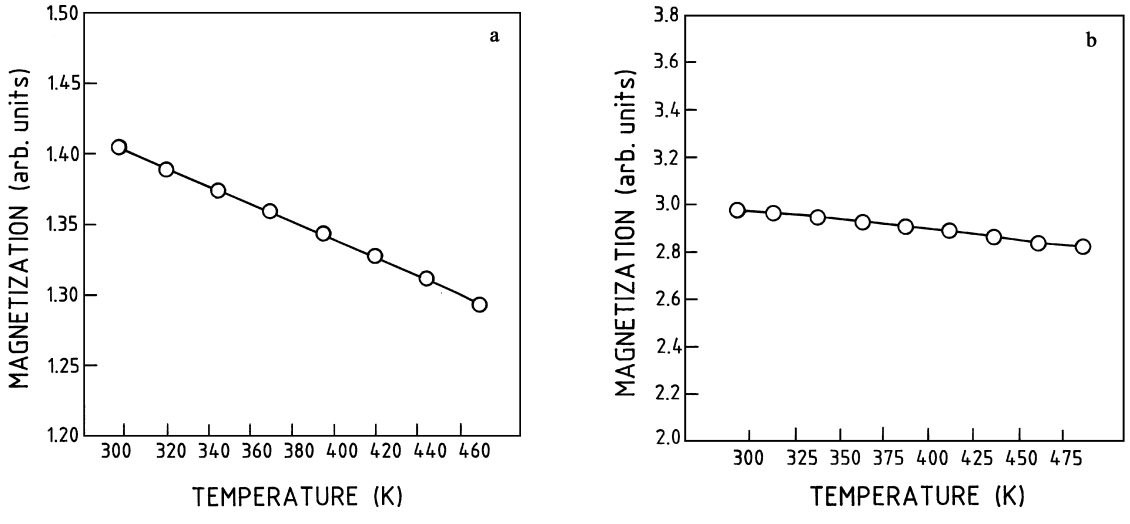

Figure 15 The plots of magnetisation as a function of temperature for thermally stabilized: (a) normal 2:17 and (b) Gd-substituted 2:17 samples.

where, P1 and P2 are the values of magnetisation at temperatures T1 and T2 respectively and ppm represents parts per million.

The values calculated between 30–200°C for the normal 2:17 and the Gd-substituted 2:17 samples are 400 ppm/°C and 350 ppm/°C respectively and those estimated over the temperature range of 30–100°C are 350 ppm/°C and 225 ppm/°C respectively.

4. Summary

From the microstructural and magnetic investigations in 2:17 type SmCo samples with and without Gd-substitution, the following inferences can be drawn:

i. Solution heat treatment at 1463 K for normal 2:17 and 1473 K for Gd-substituted 2:17 samples favored the formation of a two phase ($TbCu_7 + Th_2Zn_{17}$) structure, which appears to be a pre-requisite for achieving a large intrinsic coercivity in the magnets.

ii. A progressive variation in the proportion of the lamellar structure as a function of solution heat treatment temperature has been observed and it is found to vary significantly in the temperature range of 1463–1473 K. The XRD intensity ratio of $(204)_{2:17R}/(203)_{2:17H}$ as well as the ratio of $H_k/{}_iH_c$ as a function of solution heat treatment temperature have exhibited a maxima in the above temperature range suggesting a correlation between structure and the magnetic properties.

iii. Partial replacement of Sm by 25 wt% Gd has resulted in a reduction of energy product without affecting the intrinsic coercivity (>1300 kA/m). The temperature coefficient of magnetisation in temperature range of 30–100°C is found to be reduced from 350 to 225 ppm/°C.

Acknowledgements

The authors are grateful to Defence Research and Development Organization, New Delhi and Vikram Sarabhai Space Centre, Trivandrum for the financial support to carry out this work. The keen interest shown by the Director, DMRL in this work is also gratefully acknowledged.

References

1. T. OJIMA, S. TOMIZAWA, T. YONEYAMA and T. HORI, *IEEE Trans. Magn.* **MAG-13** (1977) 1317.
2. S. LIU and A. E. RAY, *ibid.* **MAG-25** (1989) 3785.

3. S. LIU, A. E. RAY and H. F. MILDRUM, *ibid.* **MAG-26** (1990) 1382.
4. A. E. RAY, *J. Appl. Phys.* **55** (1984) 2094.
5. G. C. HADJIPANAYIS, E. J. YADLOWSKY and S. H. WOLLINS, *ibid.* **53** (1982) 2386.
6. L. RABENBERG, R. K. MISHRA and G. THOMAS, *ibid.* **53** (1982) 2389.
7. B. Y. WONG, M. WILLARD and D. E. LAUGHLIN, *J. Magn. Magn. Mater.* **169** (1997) 178.
8. J. F. LIU, Y. DING and G. C. HADJIPANAYIS, *J. Appl. Phys.* **85** (1999) 1670.
9. R. GOPALAN, K. MURALEEDHARAN, T. S. R. K. SASTRY, A.K. SINGH, V. JOSHI, D. V. SRIDHARA RAO and V. CHANDRASEKARAN, *J. Mater. Sci.* **36** (2001) 4117.
10. D. LI, E. XU, J. LIU and Y. DU, *IEEE Trans. Magn.* **MAG-16** (1980) 988.
11. H. F. MILDRUM, J. B. KRUPAR and A. E. RAY, *J. Less-Common Met.* **93** (1983) 261.
12. M. S. WALMER, C. H. CHEN, M. H. WALMER, S. LIU and G. E. KUHL, in Proc. of Rare Earth Magnet Workshop Held at Dresden, Germany (1988) p. 689.
13. K. KUMAR, *J. Appl. Phys.* **63** (1988) R13.
14. B. ZHANG, J. R. BLACHERE, W. A. SOFFA and A. E. RAY, *ibid.* **64** (1988) 5729.
15. Y. MORITA, T. UMEDA and Y. KIMURA, in Proc. of the MRS Int. Meeting on Advanced Materials, edited by M. Doyama, S. Somiya and R. P. H. Chang (Sunshine City, Ikebukura, Tokyo, Japan, 1988) Vol. 11, p. 97.
16. H. SAITO, M. TAKAHASHI, T. WAKIYAMA, G. KIDO and H. NAKAGAWA, *J. Magn. Magn. Mater.* **82** (1989) 322.
17. R. L. BERGNER, H. A. LEUPOLD, J. T. BRESLIN, F. ROTHWARF and A. TAUBER, *J. Appl. Phys.* **50** (1979) 2349.

Received 18 July 2002
and accepted 12 January 2004